Performance Analysis of RIS/STAR-IOS-Aided V2V NOMA/OMA Communications Over Composite Fading Channels

Farshad Rostami Ghadi, Masoud Kaveh, and Diego Martín

***Abstract*—In this article, we explore the communication performance of vehicle-to-vehicle (V2V) networks assisted by a reconfigurable intelligent surface (RIS) and a simultaneous transmitting and reflecting intelligent omni-surface (STAR-IOS) under non-orthogonal multiple access (NOMA) and orthogonal multiple access (OMA) schemes. In particular, we consider that the RIS is close to the transmitter vehicle while the STAR-IOS is near the receiver vehicles. In addition, it is assumed that the STAR-IOS exploits the energy-splitting (ES) protocol for communication and the fading channels between the RIS and STAR-IOS follow composite Fisher-Snedecor $\mathcal{F}$ distribution. Under such assumptions, we first use the central limit theorem (CLT) to derive the PDF and the CDF of equivalent channels at receiver vehicles, and then, we derive the closed-form expression of outage probability (OP) under NOMA/OMA scenarios. Additionally, by exploiting Jensen's inequality, we propose an upper bound of the ergodic capacity (EC) and subsequently develop an analytical expression of the energy efficiency (EE) for both NOMA and OMA cases. Further, our analytical results, which are double-checked with the Monte-Carlo simulation, reveal that applying RIS/STAR-RIS in V2V communications significantly enhances the communication performance of intelligent transportation systems (ITS). Besides, the results indicate that considering the NOMA scheme provides better performance in terms of the OP, EC, and EE as compared with the OMA case for the considered V2V communication system.**

***Index Terms*—V2V communications, RIS, STAR-IOS, NOMA, Fisher-Snedecor $\mathcal{F}$ fading, ergodic capacity, outage probability, energy efficiency.**

I. Introduction

DEVELOPMENTS in the context of intelligent transportation systems (ITSs) have led to significant attention being paid to vehicular communication in recent years [1]. Vehicular communications, often referred to as vehicle-to-everything (V2X) communications, hold significant potential for enabling advanced applications, including self-driving cars which will be provided by the sixth-generation (6G) wireless technologies [2]. Moreover, V2X communications, e.g., vehicle-to-vehicle (V2V) communications, will provide remarkable advantages such as enhancing the quality-of-service (QoS) requirements of the vehicle user equipment, improving road safety and air quality, and increasing the collective awareness of all vehicles within the immediate driving surroundings [3]. However, to achieve the above-mentioned ambitious goals in future wireless technologies such as 6G, it will be needed the incorporation of a variety of technologies, encompassing unmanned aerial vehicles (UAVs), Reconfigurable intelligent surfaces (RISs), visible light communication (VLC), edge caching, non-orthogonal multiple access (NOMA), etc. Therefore, by combining such key technologies, future 6G-V2X networks will be able to provide a smart, self-sufficient, user-controlled platform for connectivity and services in ITSs.

RIS has been recently introduced as a compelling innovation due to its ability to expand coverage range and offer exceptional spectral and energy effectiveness for 6G communications [4]. Generally speaking, RIS is an artificial metasurface with a multitude of cost-effective passive reflective components that can intelligently and adaptively enable a smart radio environment (SRE) and maximize the desired signal quality at receivers. However, one of the key limitations of RIS is that the transmitter and receiver must both be positioned on a single side of the RIS, meaning that the RIS can only support the half-space of the SRE. To address this challenge, an innovative idea of simultaneous transmitting and reflecting intelligent omni-surface (STAR-IOS) has been intriduced which is able to enable a 360° coverage region of SREs [5]. By exploiting this unique feature of STAR-IOS, separate reflection and refraction passive beamforming can be designed for the various serving regions.

Moreover, given the advantage of STAR-IOS in delivering comprehensive coverage across all spatial dimensions, there has been recently a growing interest in integrating these devices with NOMA techniques. Generally, in the NOMA approach, numerous signals are overlaid in the power dimension and concurrently transmitted within the identical frequency/time channel. Following this, the receiver employs successive interference

Manuscript received 9 November 2023; accepted 23 November 2023. Date of publication 30 November 2023; date of current version 23 February 2024. This work was supported in part by the Project PRESECREL under Grant PID2021-124502OB-C43, and in part by the Ministerio de Ciencia e Investigación (Spain), in relation to the Plan Estatal de Investigación Científica y Técnica y de Innovación 2017-2020. *(Corresponding author: Diego Martín.)*

Farshad Rostami Ghadi is with the Department of Electronic and Electrical Engineering, University College London, WC1E 6BT London, U.K. (e-mail: f.rostamighadi@ucl.ac.uk).

Masoud Kaveh is with the Department of Information and Communication Engineering, Aalto University, 02150 Espoo, Finland (e-mail: masoud.kaveh@aalto.fi).

Diego Martín is with the ETSI de Telecomunicación, Universidad Politécnica de Madrid, 28040 Madrid, Spain (e-mail: diego.martin.de.andres@upm.es).

Color versions of one or more figures in this article are available at https://doi.org/10.1109/TIV.2023.3337898.

Digital Object Identifier 10.1109/TIV.2023.3337898

elimination (SIC) to mitigate the interference induced by the superimposed coding. [6]. In this context, the pivotal element for realizing the complete benefits of NOMA systems lies in the optimal power allocation, which fulfills a critical function among users in improving the system performance. Following the power allocation guideline of the NOMA scheme, less power is assigned to users with favorable channel conditions, whereas users experiencing suboptimal channel conditions are allocated greater power. By doing so, NOMA can provide better performance compared with orthogonal multiple access (OMA) regarding substantial spectral effectiveness, extensive connectivity, and maintaining equitable user treatment [7].

A. Related Works

Great efforts have been recently carried out to study the performance of RIS/STAR-IOS-assisted V2X communications. In [8], the authors studied the power allocation problem for RIS-aided V2V communication systems based on slowly varying large-scale fading channel information. By considering an analytical framework grounded in the principles of stochastic geometry, the authors in [9] analyzed the performance of RIS-aided V2V communication networks regarding outage probability (OP), throughput, and delay outage rate (DOR). Considering the occurrence of obstacles and the density of vehicles in real-world road scenarios, the authors in [10] derived a series-form expression of the OP for a RIS-aided vehicular communication network, using the central limit theorem (CLT). By considering the low-latency and high-reliability requirements of V2V links, the authors in [11] evaluated the ergodic capacity (EC) optimization problem and derived a closed-form expression of optimal phase shifts in vehicle-to-infrastructure (V2I) communications with the help of RIS.

The authors in [12] also optimized the achievable sum-rate for a RIS-aided V2X communication system under full-duplex (FD) mode. The achievable rate for a RIS-assisted high-mobility vehicular communication system was investigated in [13], proposing a flexible two-step transmission protocol. Aiming to provide reliable and energy-efficient connectivity for autonomous vehicles, the authors in [14] optimized the placement problem of RISs over a V2X communication system. Inspired by the promise of RIS in vehicular networks, the secrecy performance metrics for RIS-aided V2V communication under Rayleigh fading channels were also analyzed in [15]. By considering an opportunistic terrestrial selection scheme over V2V communications, the authors in [16] derived the closed-form expression of the secrecy outage probability (SOP) for the integrated satellite multiple two-way terrestrial relay networks. In addition, by considering the multiple vehicle eavesdroppers, the authors in [17] analyzed the secrecy performance of the RIS-based integrated satellite UAV relay networks.

By considering a dual RIS-aided V2I communication system, the authors in [18] derived closed-form expressions of the OP, upper/lower bounds of spectral efficiency (SE), and energy efficiency (EE) under Nakagami-m fading channels. Only recently, the authors in [19] formulated an optimization problem to optimize the attainable data rate for users in a STAR-RIS-aided V2X communication system. By comparing the NOMA and OMA schemes, the OP for a STAR-RIS-aided vehicular communication was derived in [20]. In addition to aforesaid scientific efforts, several contributions have been also done to analyze the various performance metrics of STAR-RIS-aided NOMA communications in recent years [21], [22], [23], [24], [25], [26]. However, previous works did not consider RIS and STAR-IOS in vehicular networks simultaneously to analyze the system important performance metrics.

B. Motivation and Contributions

Motivated by the aforesaid advantages of RIS and STAR-IOS techniques in intelligent practical applications of future wireless networks, e.g., 6G, as well as the inherent potential of the NOMA scheme in providing higher SE over various communication systems, in this article, we integrate the emerging RIS and STAR-IOS technologies to analyze the performance of vehicular networks, e.g., V2V communication systems, under OMA and NOMA schemes. To the best of the author's knowledge, there has been no previous work that exploits the RIS and STAR-RIS simultaneously to evaluate V2X communications under composite fading channels. Most previous contributions considered the RIS, STAR-IOS, or dual RIS separately in their proposed system model, however, the impact of the cooperation between RIS and STAR-IOS on the system performance remains unanswered so far.

To this end, in particular, we consider a V2V communication, where a transmitter vehicle wants to send an independent message to vehicle receivers with the help of RIS and STAR-IOS which are located close to the transmitter and receivers, respectively. Besides, in order to accurately model the statistical characteristics of fading channel coefficients, we assume that the channels between the RIS and STAR-IOS undergo Fisher-Snedecor $\mathcal{F}$ distribution. Moreover, after determining the marginal distributions of the equivalent channel at the receivers by exploiting the CLT, we derive analytical expressions of important performance metrics in wireless communications, and then, we evaluate the efficiency of the proposed system model in terms of derived metrics. Thus, the main contributions of our work are summarized as follows

- By utilizing the CLT, we first obtain analytical expressions of the cumulative distribution function (CDF) and probability density function (PDF) for the signal-to-noise ratio (SNR) at the receiver vehicles.
- Then, by exploiting the provided CDF and PDF, we derive the closed-form expression of the OP, a tight upper bound of ergodic capacity (EC), and the analytical expression of EE for both OMA and NOMA schemes under Fisher-Snedecor $\mathcal{F}$ fading channels.
- Eventually, we assess the performance of the analyzed RIS/STAR-IOS system with a focus on the OP, EC, and EE. To do so, we double-check the accuracy of our analytical expressions with Monte-Carlo simulation, where the numerical results confirm that considering RIS/STAR-IOS in V2V communications is quite beneficial for the system

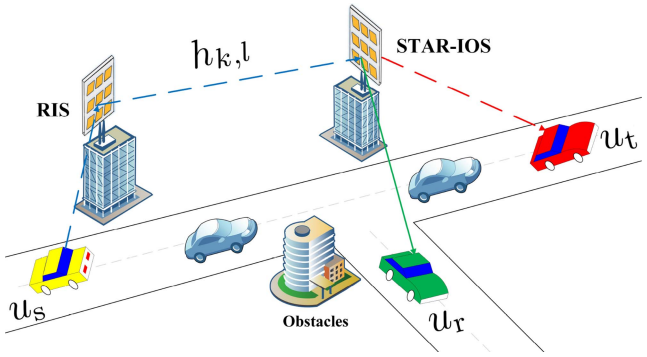

Fig. 1. Illustration of RIS/STAR-IOS-aided V2V communications.

performance and that the use of NOMA provides better performance in comparison with the OMA counterpart.

II. System Model

A. Channel Model

We consider a wireless V2V NOMA communication scenario as shown in Fig. 1, wherein a transmitter vehicle $u_{\rm s}$ aims to communicate information with other receiver vehicles $u_{\rm w}$, ${\rm w} \in \{{\rm r}, {\rm t}\}$ which are located in the reflection and refraction regions. We assume that the direct links between the vehicle transmitter $u_{\rm s}$ and the vehicle receivers $u_{\rm w}$ are blocked due to obstacles. Hence, we consider a RIS with N_1 elements and a STAR-IOS with N_2 elements to support this transmission, one each placed near the transmitter vehicle $u_{\rm s}$ and the receiver vehicles $u_{\rm w}$, respectively. In addition, it is assumed that the distance between the transmitter vehicle and the RIS, $d_{\rm sR}$, along with the distance between the STAR-IOS and receiver vehicles, $d_{\rm Sw}$, are small, thereby, the corresponding channels can be properly modeled as deterministic line-of-sight (LoS) channels. However, by considering a large distance between the RIS and the STAR-IOS, $d_{\rm RS}$, it is presumed the quasi-static fading channels between the k-th element of RIS and the l-th element of STAR-IOS follow Fisher-Snedecor $\mathcal{F}$ distribution, i.e., $h_{k,l} \sim \mathcal{F}(m_1, m_2)$, where m_1 and m_2 are degrees of freedom which can denote the amount of shadowing of the root-mean-square (rms) signal power and the fading severity parameter, respectively. Therefore, the received signal at $u_{\rm w}$ can be respectively expressed as

$$Y_{\rm w} = \sqrt{P}\left(\sum_{k=1}^{N_1}\sum_{l=1}^{N_2}\Phi_k h_{k,l}\Psi_{{\rm w},l}\right)\left(\sqrt{p_{\rm t}}X_{\rm t} + \sqrt{p_{\rm r}}X_{\rm r}\right) + Z_{\rm w}, \tag{1}$$

in which P denotes the total transmit power, $X_{\rm w}$ defines the symbol transmitted to $u_{\rm w}$ with unit power (i.e., $\mathbb{E}[|X_{\rm w}|^2]$), $p_{\rm w}$ is the power allocation factor for $u_{\rm w}$, so that $p_{\rm t} + p_{\rm r} = 1$, and $Z_{\rm w}$ is the additive white Gaussian noise (AWGN) with zero mean and variance σ_n^2 at $u_{\rm w}$. The term $h_{k,l} = \eta_{k,l} d_{\rm R,S}^{-\kappa} {\rm e}^{-j\zeta_{k,l}}$ denotes the fading channel between the RIS and the STAR-IOS, in which $\kappa > 2$, $\eta_{k,l}$, and $\zeta_{k,l}$ are the path-loss exponent, the amplitude of $h_{k,l}$, and the phase of $h_{k,l}$, respectively. Additionally, the term $\Phi_k = {\rm e}^{j\phi_k}$ contains ϕ_k which indicates the modifiable phase caused by the k-th reflecting element of the RIS. By assuming the energy-splitting protocol for the considered STAR-IOS model, all elements of the STAR-IOS simultaneously operate refraction and reflection modes, while the total radiation energy is split into two parts, i.e., $\Psi_{{\rm w},l} = \beta_{{\rm w},l}{\rm e}^{j\psi_{{\rm w},l}}$, where $\psi_{{\rm w},l}$ denotes the adjustable phases induced by the l-th element of the STAR-IOS during refraction and reflection, whereas $\beta_{{\rm w},l}$ denote the adjustable refraction/reflection coefficients of the STAR-IOS, with $\beta_{{\rm r},l}^2 + \beta_{{\rm t},l}^2 \leq 1$. To simplify the system and reduce complexity, we assume throughout the following analysis that all elements possess identical amplitude coefficients, i.e., $\beta_{{\rm w},l} = \beta_{\rm w}$, $\forall l = 1, \ldots, N_2$. Moreover, we consider the term $\mathcal{D}$ as the distance-dependent path-loss for LoS which can be defined, for a link distance d, at the carrier frequency of 3 GHz as follows [27]

$$\mathcal{D}(d)\,[dB] = -37.5 - 22\log_{10}(d/1{\rm m})\,. \tag{2}$$

B. Multiple Access Schemes

1) NOMA: As per the principles of NOMA, the transmitter vehicle $u_{\rm s}$ sends the signals of both receiver vehicles using the same time and frequency resources by superposition coding. Besides, the NOMA vehicle with a better channel condition conducts successive interference cancellation (SIC), while another vehicle decodes its signal directly treating interference as noise. Without loss of generality, as the STAR-IOS can adapt the energy allocation coefficients $\beta_{{\rm w},l}$ using the ES protocol, we designate a higher energy allocation for reflecting links, and thus, the strong receiver vehicle $u_{\rm r}$ operates the SIC process. This implies in turn that the receiver vehicle in the refraction zone $u_{\rm t}$ is allocated more power by the transmitter vehicle (i.e., $p_{\rm r} < p_{\rm t}$). Therefore, the signal-to-interference-plus-noise ratio (SINR) of the SIC process for $u_{\rm r}$ can be expressed as

$$\gamma_{\rm sic} = \frac{\bar{\gamma}p_{\rm t}\beta_{\rm r}^2\mathcal{D}d_{\rm RS}^{-\kappa}\left|\sum_{k=1}^{N_1}\sum_{l=1}^{N_2}\eta_{k,l}{\rm e}^{j(\phi_k+\psi_{{\rm r},l}-\zeta_{k,l})}\right|^2}{\bar{\gamma}p_{\rm r}\beta_{\rm r}^2\mathcal{D}d_{\rm RS}^{-\kappa}\left|\sum_{k=1}^{N_1}\sum_{l=1}^{N_2}\eta_{k,l}{\rm e}^{j(\phi_k+\psi_{{\rm r},l}-\zeta_{k,l})}\right|^2 + 1}, \tag{3}$$

where $\bar{\gamma} = \frac{P}{\sigma_n^2}$ is the transmit SNR. Then, with the aid of SIC, $u_{\rm r}$ removes the message of $u_{\rm t}$ from its received signal and decodes its required information with the following SNR

$$\gamma_{\rm r}^{\rm n} = \bar{\gamma}p_{\rm r}\beta_{\rm r}^2\mathcal{D}d_{\rm RS}^{-\kappa}\left|\sum_{k=1}^{N_1}\sum_{l=1}^{N_2}\eta_{k,l}{\rm e}^{j(\phi_k+\psi_{{\rm r},l}-\zeta_{k,l})}\right|^2. \tag{4}$$

Simultaneously, $u_{\rm t}$ directly decodes its signal by considering the signal of $u_{\rm r}$ as interference. Thus, the SINR at $u_{\rm t}$ can be expressed as

$$\gamma_{\rm t}^{\rm n} = \frac{\bar{\gamma}p_{\rm t}\beta_{\rm t}^2\mathcal{D}d_{\rm RS}^{-\kappa}\left|\sum_{k=1}^{N_1}\sum_{l=1}^{N_2}\eta_{k,l}{\rm e}^{j(\phi_k+\psi_{{\rm t},l}-\zeta_{k,l})}\right|^2}{\bar{\gamma}p_{\rm r}\beta_{\rm t}^2\mathcal{D}d_{\rm RS}^{-\kappa}\left|\sum_{k=1}^{N_1}\sum_{l=1}^{N_2}\eta_{k,l}{\rm e}^{j(\phi_k+\psi_{{\rm t},l}-\zeta_{k,l})}\right|^2 + 1}. \tag{5}$$

2) OMA: Conversely, the SNR at user $u_{\rm w}$ in OMA, such as time division multiple access (TDMA), can be defined as

$$\gamma_{\rm w}^{\rm o} = \bar{\gamma}\mathcal{D}d_{\rm RS}^{-\kappa}\beta_{\rm w}^2\left|\sum_{k=1}^{N_1}\sum_{l=1}^{N_2}\eta_{k,l}{\rm e}^{j(\phi_k+\psi_{{\rm w},l}-\zeta_{k,l})}\right|^2. \quad (6)$$

3) Phase Adjustment: Here, by adjusting the phase at the RIS-to-STAR-IOS channel to cancel the resultant phase, i.e., $\zeta_{k,l} = \phi_k + \psi_{{\rm w},l}$, the SNR at receiver vehicles $u_{\rm w}$ can be maximized. Therefor, by defining the random variable (RV) $V = |\sum_{k=1}^{N_1}\sum_{l=1}^{N_2}\eta_{k,l}|$, the maximum SNR at $u_{\rm w}$ can be obtained under an ideal phase shift for both NOMA and OMA schemes.

III. Performance Analysis

Here, we first introduce the marginal distributions of the SNRs at each users, and then, we derive the closed-form expressions of the OP, EC, and EE under Fisher-Snedecor $\mathcal{F}$ fading channels.

A. Statistical Characterization

By exploiting the CLT when $N_1, N_2 \gg 1$, the RV V can be accurately estimated by a Gaussian distribution with the following marginal PDF and CDF, respectively

$$f_V(v) = \frac{1}{\sqrt{2\pi\sigma_{\rm V}^2}}\exp\left(-\frac{(v-\mu_V)^2}{2\sigma_{\rm V}^2}\right), \quad v>0 \quad (7)$$

$$F_V(v) = 1 - {\rm Q}\left(\frac{v-\mu_V}{\sigma_V^2}\right), \quad v>0 \quad (8)$$

where $Q(.)$ denotes the Q-function. The terms $\sigma_V^2 = \sum_{k=1}^{N_1}\sum_{l=1}^{N_2}\sigma_{k,l}^2$ and $\mu_V = \sum_{k=1}^{N_1}\sum_{l=1}^{N_2}\mu_{k,l}$ are the mean and variance of the RV V, respectively. Moreover, $\mu_{k,l} = \frac{m_2}{m_2-1}$ and $\sigma_{k,l}^2 = \frac{m_2^2(m_1+m_2-1)}{m_1(m_2-1)^2(m_2-2)}$ are the mean and variance of the RV $\eta_{k,l}$ for all $k = \{1,\ldots,N_1\}$ and $l = \{1,\ldots,N_2\}$, respectively, which undergoes the Fisher-Snedecor $\mathcal{F}$ distribution.

B. Outage Probability

OP serves as a suitable metric for assessing the effectiveness of wireless communication systems and is defined as the probability that the random SNR γ is less than an SNR threshold $\gamma_{\rm th}$, i.e.,

$$P_{\rm out} = \Pr\left(\gamma \le \gamma_{\rm th}\right). \quad (9)$$

Proposition 1: The OP over the considered dual RIS/STAR-IOS-aided V2V NOMA communications for the receiver vehicles $u_{\rm t}$ and $u_{\rm r}$ can be respectively given by

$$P_{\rm t,out}^{\rm n} = 1 - {\rm Q}\left(\frac{\breve{\gamma}_{\rm t} - N_1N_2\frac{m_2}{m_2-1}}{N_1N_2\frac{m_2^2(m_1+m_2-1)}{m_1(m_2-1)^2(m_2-2)}}\right), \quad (10)$$

$$P_{\rm r,out}^{\rm n} = \left[1 - {\rm Q}\left(\frac{\hat{\gamma}_{\rm sic} - N_1N_2\frac{m_2}{m_2-1}}{N_1N_2\frac{m_2^2(m_1+m_2-1)}{m_1(m_2-1)^2(m_2-2)}}\right)\right] \times \left[1 - {\rm Q}\left(\frac{\breve{\gamma}_{\rm r} - N_1N_2\frac{m_2}{m_2-1}}{N_1N_2\frac{m_2^2(m_1+m_2-1)}{m_1(m_2-1)^2(m_2-2)}}\right)\right], \quad (11)$$

where $\breve{\gamma}_{\rm t} = \sqrt{\frac{\bar{\gamma}_{\rm t}^{\rm n}}{\bar{\gamma}\beta_{\rm t}^2\mathcal{D}d_{\rm RS}^{-\kappa}(p_{\rm t}-p_{\rm r}\bar{\gamma}_{\rm t}^{\rm n})}}$, $\hat{\gamma}_{\rm sic} = \sqrt{\frac{\bar{\gamma}_{\rm sic}}{\bar{\gamma}\beta_{\rm r}^2\mathcal{D}d_{\rm RS}^{-\kappa}(p_{\rm r}-p_{\rm t}\bar{\gamma}_{\rm sic})}}$, and $\breve{\gamma}_{\rm r} = \sqrt{\frac{\bar{\gamma}_{\rm r}^{\rm n}}{\bar{\gamma}\beta_{\rm r}^2p_{\rm r}\mathcal{D}d_{\rm RS}^{-\kappa}}}$. Besides, $\breve{\gamma}_{\rm t}$, $\hat{\gamma}_{\rm sic}$, and $\breve{\gamma}_{\rm r}$ are the SNR thresholds of $\gamma_{\rm t}$, $\gamma_{\rm sic}$, and $\gamma_{\rm r}$, respectively.

Proof: Regarding the principle of NOMA, the outage occurs at $u_{\rm r}$ when it cannot decode the signal of $u_{\rm t}$ or its own signal, or both. Hence, the OP of $u_{\rm r}$ is defined as

$$P_{\rm r,out}^{\rm n} = \Pr\left(\gamma_{\rm sic} \le \bar{\gamma}_{\rm sic}, \gamma_{\rm r}^{\rm n} \le \bar{\gamma}_{\rm r}^{\rm n}\right), \quad (12)$$

where $\bar{\gamma}_{\rm sic}$ and $\bar{\gamma}_{\rm r}^{\rm n}$ are the corresponding SINR/SNR thresholds. In this case, it should be noted that the OP highly depends on the relation between power allocation factors $p_{\rm r}$ and $p_{\rm t}$. Hence, when $p_{\rm t} \le \bar{\gamma}_{\rm sic}p_{\rm r}$, we will have $P_{\rm r,out}^{\rm n} = 1$; Otherwise, when $p_{\rm t} > \bar{\gamma}_{\rm sic}p_{\rm r}$, by considering the ideal phase shift to reach the maximum received signal, and then, inserting (3) and (4) into (12), the OP of $u_{\rm r}$ can be given by

$$P_{\rm r,out}^{\rm n} \overset{(a)}{=} \Pr\left(\frac{\bar{\gamma}p_{\rm r}\mathcal{D}d_{\rm RS}^{-\kappa}\beta_{\rm r}^2V^2}{\bar{\gamma}p_{\rm t}\mathcal{D}d_{\rm RS}^{-\kappa}\beta_{\rm r}^2V^2+1} \le \bar{\gamma}_{\rm sic}\right) \times \Pr\left(\bar{\gamma}p_{\rm r}\mathcal{D}d_{\rm RS}^{-\kappa}\beta_{\rm r}^2V^2 \le \bar{\gamma}_{\rm r}^{\rm n}\right) \quad (13)$$

$$= \Pr\left(V \le \sqrt{\frac{\bar{\gamma}_{\rm sic}}{\bar{\gamma}\beta_{\rm r}^2\mathcal{D}d_{\rm RS}^{-\kappa}\left(p_{\rm r}-p_{\rm t}\bar{\gamma}_{\rm sic}\right)}}\right) \times \Pr\left(V \le \sqrt{\frac{\bar{\gamma}_{\rm r}^{\rm n}}{\bar{\gamma}p_{\rm r}\mathcal{D}d_{\rm RS}^{-\kappa}\beta_{\rm r}^2}}\right) \quad (14)$$

$$= F_V\left(\hat{\gamma}_{\rm sic}\right)F_V\left(\breve{\gamma}_{\rm r}\right) \quad (15)$$

$$= \left[1 - {\rm Q}\left(\frac{\hat{\gamma}_{\rm sic}-\mu_V}{\sigma_V^2}\right)\right]\left[1 - {\rm Q}\left(\frac{\breve{\gamma}_{\rm r}-\mu_V}{\sigma_V^2}\right)\right], \quad (16)$$

where (a) is obtained from the independence of the events. Next, by substituting the values of μ_V and σ_V^2 that previously obtained, the proof of $P_{\rm r,out}^{\rm n}$ is accomplished.

As for the proof of $P_{\rm t,out}^{\rm n}$, the outage is said to happen for $u_{\rm t}$ when its received SINR $\gamma_{\rm t}^{\rm n}$ drops below a certain SINR threshold $\bar{\gamma}_{\rm t}^{\rm n}$, i.e.,

$$P_{\rm t,out}^{\rm n} = \Pr\left(\gamma_{\rm t}^{\rm n} \le \bar{\gamma}_{\rm t}^{\rm n}\right). \quad (17)$$

Now, using analogous procedures as in the analysis of $u_{\rm r}$, under the case of $p_{\rm t} \le \bar{\gamma}_{\rm t}^{\rm n}p_{\rm r}$, we will have $P_{\rm t,out}^{\rm n} = 1$. However, when $p_{\rm t} > \bar{\gamma}_{\rm t}^{\rm n}p_{\rm r}$, by inserting (5) into (17), the OP of $u_{\rm t}$ can be given by

$$P_{\rm t,out}^{\rm n} = \Pr\left(\frac{\bar{\gamma}p_{\rm t}\mathcal{D}d_{\rm RS}^{-\kappa}\beta_{\rm t}^2V^2}{\bar{\gamma}p_{\rm r}\mathcal{D}d_{\rm RS}^{-\kappa}\beta_{\rm t}^2V^2+1} \le \bar{\gamma}_{\rm t}^{\rm n}\right) \quad (18)$$

$$= \Pr\left(V \le \sqrt{\frac{\bar{\gamma}_{\rm t}^{\rm n}}{\bar{\gamma}\beta_{\rm t}^2\mathcal{D}d_{\rm RS}^{-\kappa}\left(p_{\rm t}-p_{\rm r}\bar{\gamma}_{\rm t}^{\rm n}\right)}}\right) \quad (19)$$

$$= F_V\left(\breve{\gamma}_{\rm t}\right) = 1 - {\rm Q}\left(\frac{\breve{\gamma}_{\rm w}-\mu_V}{\sigma_V^2}\right), \quad (20)$$

now, by substituting the values of μ_V and σ_V^2 that previously obtained, the proof of $P_{\mathrm{t,out}}^{\mathrm{n}}$ is completed. □

Proposition 2: The OP over the considered dual RIS/STAR-IOS-aided V2V OMA communications for the receiver vehicles u_{w} can be given by

$$P_{\mathrm{w,out}}^{\mathrm{o}} = 1 - \mathrm{Q}\left(\frac{\tilde{\gamma}_{\mathrm{w}} - N_1 N_2 \frac{m_2}{m_2-1}}{N_1 N_2 \frac{m_2^2(m_1+m_2-1)}{m_1(m_2-1)^2(m_2-2)}}\right), \tag{21}$$

where $\tilde{\gamma}_{\mathrm{w}} = \sqrt{\frac{\bar{\gamma}_{\mathrm{w}}^{\mathrm{o}}}{\bar{\gamma}\mathcal{D}d_{\mathrm{RS}}^{-\kappa}\beta_{\mathrm{w}}^2}}$ and $\bar{\gamma}_{\mathrm{w}}^{\mathrm{o}}$ denotes the SNR threshold of u_{w}.

Proof: As for the OMA scheme, the OP of receiver vehicles u_{w} can be characterized as the likelihood that $\gamma_{\mathrm{w}}^{\mathrm{o}}$ less than the SNR threshold $\bar{\gamma}_{\mathrm{w}}^{\mathrm{o}}$, i.e.,

$$P_{\mathrm{w,out}}^{\mathrm{o}} = \Pr\left(\gamma_{\mathrm{w}} \leq \bar{\gamma}_{\mathrm{w}}^{\mathrm{o}}\right). \tag{22}$$

Next, by plugging (6) into (22) and considering the ideal phase shift, we have

$$P_{\mathrm{w,out}}^{\mathrm{o}} = \Pr\left(V \leq \sqrt{\frac{\bar{\gamma}_{\mathrm{w}}^{\mathrm{o}}}{\bar{\gamma}\mathcal{D}d_{\mathrm{RS}}^{-\kappa}\beta_{\mathrm{w}}^2}}\right) \tag{23}$$

$$= F_V\left(\tilde{\gamma}_{\mathrm{w}}\right) = 1 - \mathrm{Q}\left(\frac{\tilde{\gamma}_{\mathrm{w}} - \mu_V}{\sigma_V^2}\right). \tag{24}$$

Now, by substituting the values of μ_V and σ_V^2 that previously obtained, the proof of $P_{\mathrm{w,out}}^{\mathrm{o}}$ is completed. □

C. Ergodic Capacity

The EC for the considered system model under NOMA/OMA schemes with the instantaneous SNR $\gamma_{\mathrm{w}}^{\mathrm{z}}$, $\mathrm{z} \in \{\mathrm{n}, \mathrm{o}\}$, can be defined as

$$\bar{C}_{\mathrm{w}}^{\mathrm{z}} = \mathbb{E}\left[\log_2\left(1+\gamma_{\mathrm{w}}^{\mathrm{z}}\right)\right] = \int_0^{\infty} \log_2\left(1+\gamma_{\mathrm{w}}^{\mathrm{z}}\right) f_V(v) dv. \tag{25}$$

In general, it is mathematically intractable to derive the closed-form expression of $\bar{C}_{\mathrm{w}}^{\mathrm{z}}$. Hence, by exploiting the Jensen's inequality, we derive tight upper bound $\bar{C}_{\mathrm{w,U}}^{\mathrm{z}}$ for the EC, i.e., $\bar{C}_{\mathrm{w}}^{\mathrm{z}} \leq \bar{C}_{\mathrm{w,U}}^{\mathrm{z}}$.

Proposition 3: The upper bound EC over the considered dual RIS/STAR-IOS-aided V2V NOMA communications for the receiver vehicles u_{r} and u_{t} can be respectively given by (26) and (27) shown at the bottom of this page.

Proof: By inserting (4) and (7) into (25) and applying the Jensen's inequality, the upper bound EC of u_{r} under NOMA scheme can be defined as

$$\bar{C}_{\mathrm{r,U}}^{\mathrm{n}} = \log_2\left(1 + \bar{\gamma} p_{\mathrm{r}} \mathcal{D} d_{\mathrm{RS}}^{-\kappa} \beta_{\mathrm{r}}^2 \mathbb{E}\left[V^2\right]\right), \tag{28}$$

in which $\mathbb{E}[V^2]$ can be determined as

$$\mathbb{E}\left[V^2\right] = \mathrm{Var}\left[V\right] + \mathbb{E}^2\left[V\right] = \sigma_V^2 + \mu_V^2. \tag{29}$$

$$= N_1 N_2 \left[\frac{m_2}{m_2-1} + \frac{m_2^2\left(m_1+m_2-1\right)}{m_1\left(m_2-1\right)^2\left(m_2-2\right)}\right]. \tag{30}$$

Now, by substituting the value of $\mathbb{E}[V^2]$ into (28), $\bar{C}_{\mathrm{r,U}}^{\mathrm{o}}$ is derived as (26).

Similarly, by plugging (5) and (7) into (25) and considering the Jensen's inequality, the upper bound EC of u_{t} under NOMA case can be expressed as

$$\bar{C}_{\mathrm{t,U}}^{\mathrm{n}} = \log_2\left(1 + \frac{\bar{\gamma} p_{\mathrm{t}} \mathcal{D} d_{\mathrm{RS}}^{-\kappa} \beta_{\mathrm{t}}^2 \mathbb{E}\left[V^2\right]}{\bar{\gamma} p_{\mathrm{r}} \mathcal{D} d_{\mathrm{RS}}^{-\kappa} \beta_{\mathrm{t}}^2 \mathbb{E}\left[V^2\right] + 1}\right), \tag{31}$$

in which by inserting the values of $\mathbb{E}[V^2]$ from (30) into (31), the proof is completed. □

Proposition 4: The upper bound EC over the considered dual RIS/STAR-IOS-aided V2V OMA communications for the receiver vehicles u_{w} can be given by (32) shown at the bottom of the next page.

Proof: By inserting (6) and (7) into (25) and applying the Jensen's inequality, the upper bound EC of u_{w} under OMA scheme can be defined as

$$\bar{C}_{\mathrm{w,U}}^{\mathrm{o}} = \log_2\left(1 + \bar{\gamma}\mathcal{D}d_{\mathrm{RS}}^{-\kappa}\beta_{\mathrm{w}}^2 \mathbb{E}\left[V^2\right]\right). \tag{33}$$

Now, by substituting (30) into (33) the proof is accomplished. □

D. Energy Efficiency

EE is a vital performance metric due to limited resources in wireless communication networks. In this regard, the EE for the considered dual RIS/STAR-IOS-aided NOMA/OMA communications is defined as the ratio of the sum of ergodic capacity at u_{w} to the corresponding total power consumption P_{tot}, i.e.,

$$\mathcal{E}^{\mathrm{z}} = \frac{\bar{C}_{\mathrm{t}}^{\mathrm{z}} + \bar{C}_{\mathrm{r}}^{\mathrm{z}}}{P_{\mathrm{tot}}} \tag{34}$$

$$= \frac{\bar{C}_{\mathrm{t}}^{\mathrm{z}} + \bar{C}_{\mathrm{r}}^{\mathrm{z}}}{P/\alpha + N_1 P_{\mathrm{R}} + N_2 P_{\mathrm{S}} + P_{\mathrm{t}} + P_{\mathrm{r}}}, \tag{35}$$

where P/α is the dynamic power consumption at transmitter vehicle u_{s} in which α indicates the drain efficiency of high-power amplifier (HPA). The terms P_{R} and P_{S} denote the power consumed by each element of the RIS and STAR-IOS, respectively. Besides, P_{t} and P_{r} are the circuit power consumption at receiver vehicles u_{t} and u_{r}, respectively.

$$\bar{C}_{\mathrm{r,U}}^{\mathrm{n}} = \log_2\left(1 + \bar{\gamma} p_{\mathrm{r}} \mathcal{D} d_{\mathrm{RS}}^{-\kappa} \beta_{\mathrm{r}}^2 N_1 N_2 \left[\frac{m_2}{m_2-1} + \frac{m_2^2\left(m_1+m_2-1\right)}{m_1\left(m_2-1\right)^2\left(m_2-2\right)}\right]\right). \tag{26}$$

$$\bar{C}_{\mathrm{t,U}}^{\mathrm{n}} = \log_2\left(1 + \frac{\bar{\gamma} p_{\mathrm{t}} \mathcal{D} d_{\mathrm{RS}}^{-\kappa} \beta_{\mathrm{t}}^2 N_1 N_2 \left[\frac{m_2}{m_2-1} + \frac{m_2^2(m_1+m_2-1)}{m_1(m_2-1)^2(m_2-2)}\right]}{\bar{\gamma} p_{\mathrm{r}} \mathcal{D} d_{\mathrm{RS}}^{-\kappa} \beta_{\mathrm{t}}^2 N_1 N_2 \left[\frac{m_2}{m_2-1} + \frac{m_2^2(m_1+m_2-1)}{m_1(m_2-1)^2(m_2-2)}\right] + 1}\right). \tag{27}$$

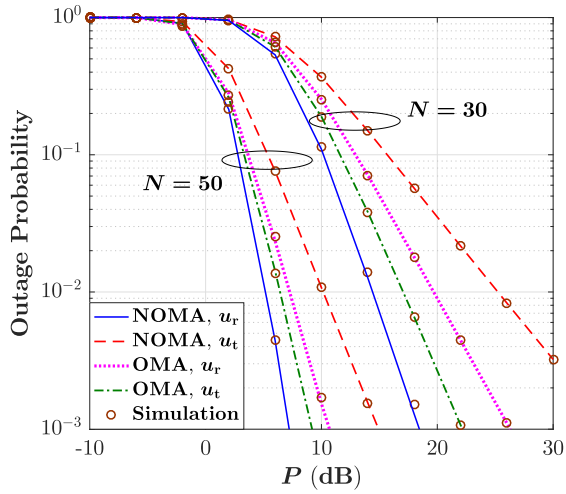

Fig. 2. OP versus transmit power P for different values of RIS/STAR-IOS elements N.

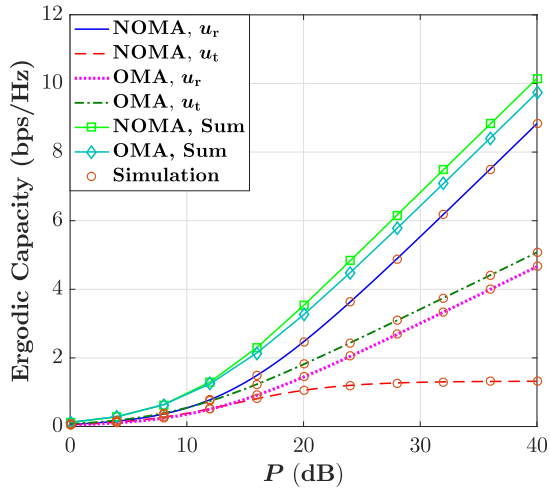

Fig. 3. EC versus transmit power P for a given value of RIS/STAR-IOS elements $N = 50$.

Here, by applying the obtained ergodic capacity of NOMA and OMA schemes to (35), the corresponding EE can be determined.

IV. Numerical Results

In this section, we provide numerical results to confirm the theoretical expressions derived earlier, and we further validate them using Monte Carlo (MC) simulations in all cases. We set the simulation parameters as $P = 30$ dBm, $\beta_{\rm r} = 0.8$, $\beta_{\rm t} = 0.6$, $p_{\rm r} = 0.4$, $p_{\rm t} = 0.6$, $d_{\rm s,R} = d_{\rm S,t} = d_{\rm S,r} = 10$ m, $\kappa = 4$, $d_{\rm RS} = 100$ m, $\sigma^2 = -90$ dBm, $\alpha = 1.2$, $P_{\rm R} = P_{\rm S} = P_{\rm t} = P_{\rm r} = 10$ dBm, and $(m_1, m_2) = (1, 3)$. In addition, for the simulation purpose, we assume that $N_1 = N_2 = N$.

Fig. 2 depicts the performance of the OP in terms of the transmit power P for different numbers of RIS/STAR-IOS reflecting elements N in the considered OMA/NOMA scenario where the channels fading model follows the Fisher-Snedecor $\mathcal{F}$ distribution. It is evident that with the growth in transmit power, the OP decreases for both receiver vehicles $u_{\rm w}$ under NOMA and OMA scenarios, which is reasonable since the channel conditions become better. We can also observe that the NOMA scheme can provide better OP performance for receiver vehicle $u_{\rm r}$ compared with the OMA case since $u_{\rm r}$ exploits the SIC in the NOMA scenario. However, it can be observed that the OP behavior for the receiver vehicle $u_{\rm t}$ improves under OMA scheme compared with the NOMA case. Moreover, it is evident that a noticeable enhancement in the OP performance of $u_{\rm w}$ is achieved with the increase in the number of RIS/STAR-IOS elements N under both OMA and NOMA case since such increment can remarkably enhance the corresponding spatial diversity.

The behavior of EC in terms of the transmit power P for a selected number of RIS/STAR-IOS elements $N = 50$ in the considered V2V OMA/NOMA communication system is illustrated in Fig. 3. In the NOMA case, we can see that the EC performance for the receiver vehicle $u_{\rm r}$ is better than that of receiver vehicle $u_{\rm t}$ across the same transmit power P, where this superiority becomes more noticeable in the high transmit power area. This behavior indicates that the EC for $u_{\rm t}$ increases linearly with P, while for $u_{\rm t}$ it converges to a constant as P increases. The main reason for these behaviors is that in the NOMA scheme u_r benefits from SIC, thereby, it has a larger SINR value compared with $u_{\rm t}$. It can be also seen that under the OMA scenario, the EC value increases continuously for both receiver vehicles $u_{\rm r}$ and $u_{\rm t}$ as the P grows. Moreover, we can notice an enhancement in the EC performance only for $u_{\rm r}$ while it deteriorates for $u_{\rm t}$ compared with the NOMA case. However, by comparing OMA and NOMA schemes, it can be seen that the NOMA case delivers a higher total system EC, highlighting its significant advantage for the considered RIS/STAR-IOS communication.

The impact of the location of RIS and STAR-IOS on the behavior of EC for a given transmit SNR $\bar{\gamma}$ is illustrated in Fig. 4. As expected, by increasing the distance between the RIS and STAR-IOS, the EC performance weakens so that for fixed values of N and $\bar{\gamma}$, the EC becomes negligible on the distance of $d_{\rm RS} = 160$ m. Fig. 5 presents more insights into the effect of the number of RIS/STAR-IOS elements on the EC performance for the considered OMA/NOMA communication system. For both OMA and NOMA schemes, it can be clearly seen that the EC performance for vehicles $u_{\rm w}$ enhances as the number of RIS/STAR-RIS elements is raised. As expected, increasing the number of RIS/STAR-IOS leads to an improvement in spatial diversity, thus, enhancing the receiver vehicles' performance. It can be also seen that increasing the average SNR $\bar{\gamma}$ provides

$$\bar{C}^{\rm o}_{\rm w,U} = \log_2\left(1 + \bar{\gamma}\mathcal{D} d_{\rm RS}^{-\kappa}\beta_{\rm w}^2 N_1 N_2 \left[\frac{m_2}{m_2 - 1} + \frac{m_2^2\left(m_1 + m_2 - 1\right)}{m_1\left(m_2 - 1\right)^2\left(m_2 - 2\right)}\right]\right). \tag{32}$$

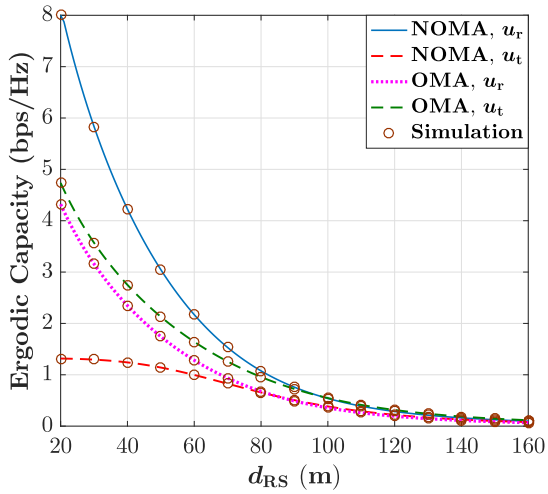

Fig. 4. EC versus the distance between RIS and STAR-IOS d_{RS} for a given value of RIS/STAR-IOS elements $N = 50$ and the transmit SNR $\bar{\gamma} = 10$ dB.

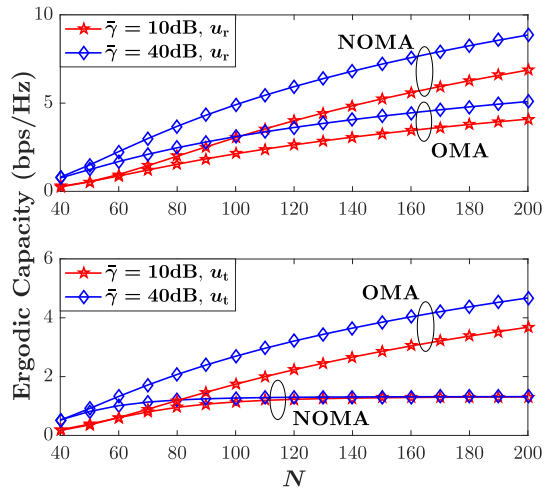

Fig. 5. EC versus the number of RIS/STAR-IOS elements N for selected values of transmit SNR $\bar{\gamma}$.

a higher EC for the vehicles u_w under both OMA and NOMA cases. Additionally, under NOMA scheme, we can observe that $\bar{\gamma}$ exerts a more pronounced influence on the EC performance of vehicle receiver u_t when N is small, however, when N increases to a certain value, $\bar{\gamma}$ does not affect the EC performance of u_t anymore. The reason for this behavior is that when N grows, the SINR of u_t reaches to a constant value, i.e., $N \to \infty, \gamma_t^n \to p_t/p_r$.

Fig. 6 shows the performance of EE in terms of the transmit power P for selected values of the number of RIS/STAR-IOS elements N under OMA and NOMA scenarios. We can see that by increasing the transmit power P, EE initially increases and reaches its highest point at approximately the value of $P = 5$dB, and then drops. This is because the EC is more dominant than power consumption before reaching the extreme point, however, this effect will reverse as P grows after reaching the extreme point. It is also observed that a higher value of EE can be provided as the number of RIS/STAR-IOS elements

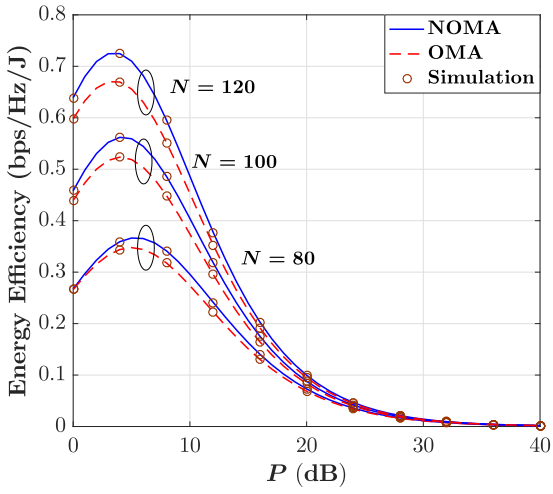

Fig. 6. EE versus the transmit power P for selected values of RIS/STAR-IOS elements N.

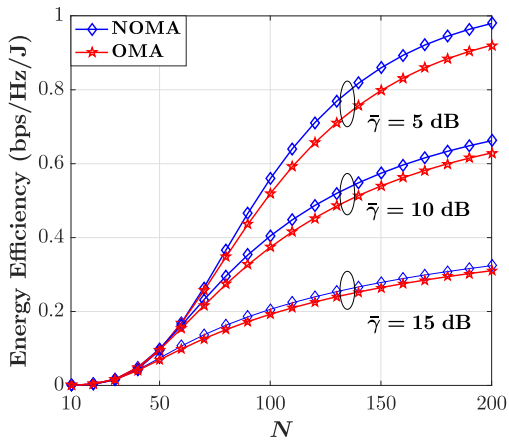

Fig. 7. EE versus the transmit power P for selected values of RIS/STAR-IOS elements N.

increases which is reasonable since the EC improves under such conditions. Furthermore, it can be obtained that the NOMA case provides a better performance in terms of EE for the considered RIS/STAR-IOS communication system compared with the OMA scheme. Moreover, Fig. 7 provides more insights into the impact of the number of reflecting elements N on the performance of the EE, where it can be observed that the EE performance conterminously improves as the number of RIS/STAR-IOS elements grows. We can also see that as the transmit SNR $\bar{\gamma}$ increases, the EE behavior for NOMA and OMA cases becomes more similar for a fixed value of N.

V. Conclusion

In this article, we integrated the RIS/STAR-IOS into vehicular networks to evaluate the performance of V2V communications. To this end, by considering the OMA and NOMA scenarios, we assumed that a transmitter vehicle wants to send an independent message with the help of RIS and STAR-IOS to receiver vehicles which are located in transmission and reflection areas. In addition, we supposed that the fading channels between

RIS and STAR-IOS followed Fisher-Snedecor $\mathcal{F}$ distribution. For the considered system model, we first introduced marginal distributions for the received SNR at receiver vehicles, and then, we obtained the closed-form expression of the OP, the upper bound of EC, and EE. Eventually, our numerical results showed that considering the RIS/STAR-IOS is beneficial for vehicular communications and it can remarkably improve the performance of ITS. Additionally, the results revealed that the NOMA scheme can provide a lower OP and higher values of EC and EE compared with the OMA scenario.

REFERENCES

[1] J. Wang, K. Zhu, and E. Hossain, "Green internet of vehicles (IoV) in the 6G era: Toward sustainable vehicular communications and networking," *IEEE Trans. Green Commun. Netw.*, vol. 6, no. 1, pp. 391–423, Mar. 2022.

[2] W. Saad, M. Bennis, and M. Chen, "A vision of 6G wireless systems: Applications, trends, technologies, and open research problems," *IEEE Netw.*, vol. 34, no. 3, pp. 134–142, May/Jun. 2020.

[3] M. Noor-A-Rahim et al., "6G for vehicle-to-everything (V2X) communications: Enabling technologies, challenges, and opportunities," *Proc. IEEE*, vol. 110, no. 6, pp. 712–734, Jun. 2022.

[4] E. Basar, M. D. Renzo, J. D. Rosny, M. Debbah, M.-S. Alouini, and R. Zhang, "Wireless communications through reconfigurable intelligent surfaces," *IEEE Access*, vol. 7, pp. 116753–116773, 2019.

[5] Y. Liu et al., "STAR: Simultaneous transmission and reflection for 360°coverage by intelligent surfaces," *IEEE Wireless Commun.*, vol. 28, no. 6, pp. 102–109, Dec. 2021.

[6] Y. Saito, Y. Kishiyama, A. Benjebbour, T. Nakamura, A. Li, and K. Higuchi, "Non-orthogonal multiple access (NOMA) for cellular future radio access," in *Proc. IEEE 77th Veh. Technol. Conf.*, 2013, pp. 1–5.

[7] Z. Chen, Z. Ding, X. Dai, and G. K. Karagiannidis, "On the application of quasi-degradation to MISO-NOMA downlink," *IEEE Trans. Signal Process.*, vol. 64, no. 23, pp. 6174–6189, Dec. 2016.

[8] Y. Chen, Y. Wang, J. Zhang, and Z. Li, "Resource allocation for intelligent reflecting surface aided vehicular communications," *IEEE Trans. Veh. Technol.*, vol. 69, no. 10, pp. 12321–12326, Oct. 2020.

[9] G. Singh, A. Srivastava, and V. A. Bohara, "Visible light and reconfigurable intelligent surfaces for beyond 5G V2X communication networks at road intersections," *IEEE Trans. Veh. Technol.*, vol. 71, no. 8, pp. 8137–8151, Aug. 2022.

[10] J. Wang, W. Zhang, X. Bao, T. Song, and C. Pan, "Outage analysis for intelligent reflecting surface assisted vehicular communication networks," in *Proc. IEEE Glob. Commun. Conf.*, 2020, pp. 1–6.

[11] X. Gu et al., "Intelligent surface aided D2D-V2X system for low-latency and high-reliability communications," *IEEE Trans. Veh. Technol.*, vol. 71, no. 11, pp. 11624–11636, Nov. 2022.

[12] S. Pala, P. Saikia, S. K. Singh, K. Singh, and C.-P. Li, "Design of RIS-assisted full duplex 6G-V2X communications," in *Proc. IEEE Wireless Commun. Netw. Conf.*, 2023, pp. 1–6.

[13] Z. Huang, B. Zheng, and R. Zhang, "Transforming fading channel from fast to slow: Intelligent refracting surface aided high-mobility communication," *IEEE Trans. Wireless Commun.*, vol. 21, no. 7, pp. 4989–5003, Jul. 2022.

[14] Y. U. Ozcan, O. Ozdemir, and G. K. Kurt, "Reconfigurable intelligent surfaces for the connectivity of autonomous vehicles," *IEEE Trans. Veh. Technol.*, vol. 70, no. 3, pp. 2508–2513, Mar. 2021.

[15] Y. Ai, F. A. P. deFigueiredo, L. Kong, M. Cheffena, S. Chatzinotas, and B. Ottersten, "Secure vehicular communications through reconfigurable intelligent surfaces," *IEEE Trans. Veh. Technol.*, vol. 70, no. 7, pp. 7272–7276, Jul. 2021.

[16] K. Guo, X. Li, M. Alazab, R. H. Jhaveri, and K. An, "Integrated satellite multiple two-way relay networks: Secrecy performance under multiple eves and vehicles with non-ideal hardware," *IEEE Trans. Intell. Veh.*, vol. 8, no. 2, pp. 1307–1318, Feb. 2023.

[17] F. Zhou, X. Li, M. Alazab, R. H. Jhaveri, and K. Guo, "Secrecy performance for RIS-based integrated satellite vehicle networks with a UAV relay and MRC eavesdropping," *IEEE Trans. Intell. Veh.*, vol. 8, no. 2, pp. 1676–1685, Feb. 2023.

[18] M. H. N. Shaikh, K. Rabie, X. Li, T. Tsiftsis, and G. Nauryzbayev, "On the Performance of Dual RIS-assisted V2I Communication under Nakagami-m Fading," in *Proc. IEEE 96th Veh. Technol. Conf.*, 2022, pp. 1–5.

[19] P. S. Aung, L. X. Nguyen, Y. K. Tun, Z. Han, and C. S. Hong, "Deep reinforcement learning based joint spectrum allocation and configuration design for STAR-RIS-assisted V2X communications," *IEEE Internet Things J.*, early access, Nov. 03, 2023, doi: 10.1109/JIOT.2023.3329893.

[20] K. Guo, R. Liu, M. Alazab, R. H. Jhaveri, X. Li, and M. Zhu, "STAR-RIS-Empowered cognitive non-terrestrial vehicle network with NOMA," *IEEE Trans. Intell. Veh.*, vol. 8, no. 6, pp. 3735–3749, Jun. 2023.

[21] C. Zhang, W. Yi, Y. Liu, Z. Ding, and L. Song, "STAR-IOS aided NOMA networks: Channel model approximation and performance analysis," *IEEE Trans. Wireless Commun.*, vol. 21, no. 9, pp. 6861–6876, Sep. 2022.

[22] T. Wang, M.-A. Badiu, G. Chen, and J. P. Coon, "Outage probability analysis of STAR-RIS assisted NOMA network with correlated channels," *IEEE Commun. Lett.*, vol. 26, no. 8, pp. 1774–1778, Aug. 2022.

[23] C. Wu, Y. Liu, X. Mu, X. Gu, and O. A. Dobre, "Coverage characterization of STAR-RIS networks: NOMA and OMA," *IEEE Commun. Lett.*, vol. 25, no. 9, pp. 3036–3040, Sep. 2021.

[24] F. R. Ghadi, F. J. López-Martinez, and K.-K. Wong, "Analytical characterization of coverage regions for STAR-RIS-aided NOMA/OMA communication systems," *IEEE Commun. Lett.*, vol. 27, no. 11, pp. 3063–3067, Nov. 2023.

[25] M. Aldababsa, A. Khaleel, and E. Basar, "STAR-RIS-NOMA networks: An error performance perspective," *IEEE Commun. Lett.*, vol. 26, no. 8, pp. 1784–1788, Aug. 2022.

[26] H. Liu, G. Li, X. Li, Y. Liu, G. Huang, and Z. Ding, "Effective capacity analysis of STAR-RIS-assisted NOMA networks," *IEEE Wireless Commun. Lett.*, vol. 11, no. 9, pp. 1930–1934, Sep. 2022.

[27] E. Björnson, Ö. Özdogan, and E. G. Larsson, "Intelligent reflecting surface versus decode-and-forward: How large surfaces are needed to beat relaying?," *IEEE Wireless Commun. Lett.*, vol. 9, no. 2, pp. 244–248, Feb. 2020.

Farshad Rostami Ghadi received the Ph.D. (Hons.) degree in electrical communication systems engineering from the Ferdowsi University of Mashhad, Mashhad, Iran, in 2021. In 2021, he was a Postdoctoral Research Fellow with the Department of Communication Engineering, University of Malaga, Malaga, Spain. He is currently a Research Fellow with the Department of Electronic and Electrical Engineering, University College London, London, U.K. His research interests include analyzing wireless communication networks, network information theory, and Copula theory, with an emphasis on wireless channel modeling and physical layer security.

Masoud Kaveh received the Ph.D. degree in electrical engineering from the Iran University of Science and Technology, Tehran, Iran, in 2021. In 2020, he was a Visiting Scholar with the Technical University of Madrid, Madrid, Spain, under the Erasmus+ Program of the European Union. He is currently a postdoctoral Researcher with Aalto University, Espoo, Finland. His research interests include physical layer security, physical unclonable functions (PUFs), applied cryptography, smart grid security, backscatter communication, FPGA design, cryptographic protocols, and machine learning.

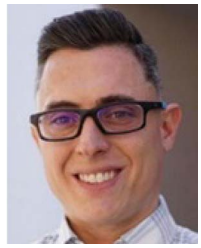

Diego Martín received the B.Sc. degree in computer engineering, the M.Sc. degree in computer science from the Department of Informatics, Carlos III University of Madrid, Madrid, Spain. He received the Ph.D. degree from the Department of Informatics, Carlos III University of Madrid, in 2012. He is currently a Lecturer with the Department of Telematics, Technical University of Madrid (UPM), Madrid. His research interests during his collaborations in the STRAST and GISAI research groups, at UPM, are Internet of Things, cyberphysical systems, physically unclonable functions, blockchain, knowledge management, information retrieval, and research methods.